The SDSS spectroscopic catalogue of white dwarf-main-sequence binaries: new identifications from DR 9–12

A. Rebassa-Mansergas,[1]★ J. J. Ren,[2] S. G. Parsons,[3] B. T. Gänsicke,[4] M. R. Schreiber,[3,5] E. García-Berro,[1,6] X.-W. Liu[2,7] and D. Koester[8]

[1]*Departament de Física, Universitat Politècnica de Catalunya, c/Esteve Terrades 5, E-08860 Castelldefels, Spain*
[2]*Department of Astronomy, Peking University, Beijing 100871, P. R. China*
[3]*Instituto de Física y Astronomía, Universidad de Valparaíso, Avenida Gran Bretaña 1111, Valparaíso, Chile*
[4]*Department of Physics, University of Warwick, Coventry CV4 7AL, UK*
[5]*Millenium Nucleus 'Protoplanetary Disks in ALMA Early Science', Universidad de Valparaíso, Avenida Gran Bretaña 1111, Valparaíso, Chile*
[6]*Institute for Space Studies of Catalonia, c/Gran Capità 2–4, Edif. Nexus 201, E-08034 Barcelona, Spain*
[7]*Kavli Institute for Astronomy and Astrophysics, Peking University, Beijing 100871, P. R. China*
[8]*Institut für Theoretische Physik und Astrophysik, University of Kiel, D-24098 Kiel, Germany*

ABSTRACT

We present an updated version of the spectroscopic catalogue of white dwarf-main-sequence (WDMS) binaries from the Sloan Digital Sky Survey (SDSS). We identify 938 WDMS binaries within the data releases (DR) 9–12 of SDSS plus 40 objects from DR 1–8 that we missed in our previous works, 646 of which are new. The total number of spectroscopic SDSS WDMS binaries increases to 3294. This is by far the largest and most homogeneous sample of compact binaries currently available. We use a decomposition/fitting routine to derive the stellar parameters of all systems identified here (white dwarf effective temperatures, surface gravities and masses, and secondary star spectral types). The analysis of the corresponding stellar parameter distributions shows that the SDSS WDMS binary population is seriously affected by selection effects. We also measure the Na I $\lambda\lambda$ 8183.27, 8194.81 absorption doublet and H α emission radial velocities (RV) from all SDSS WDMS binary spectra identified in this work. 98 objects are found to display RV variations, 62 of which are new. The RV data are sufficient enough to estimate the orbital periods of three close binaries.

Key words: binaries: close – binaries: spectroscopic – stars: low-mass – white dwarfs.

1 INTRODUCTION

A large fraction of main-sequence stars are found in binary systems (Duquennoy & Mayor 1991; Raghavan et al. 2010; Yuan et al. 2015b). It is expected that ∼25 per cent of all main-sequence binaries are close enough to begin mass transfer interactions when the more massive star becomes a red giant or an asymptotic giant star (Willems & Kolb 2004). This has been observationally verified e.g. by Farihi, Hoard & Wachter (2010) and by Nebot Gómez-Morán et al. (2011). Because the mass transfer rate generally exceeds the Eddington limit, the secondary star is not able to accrete the transferred material and the system evolves through a common envelope phase. That is, the core of the giant and the main-sequence companion orbit within a common envelope formed by the outer layers of the giant star. Drag forces between the two stars and the envelope lead to the shrinkage of the orbit and therefore to the release

of orbital energy. The orbital energy is deposited into the envelope and is eventually used to eject it (Webbink 2008). The outcome of common envelope evolution is hence a close binary formed by the core of the giant star (which later becomes a white dwarf) and a main-sequence companion, i.e. a close white dwarf-main-sequence (WDMS) binary. These are commonly referred to as post-common envelope binaries (PCEBs). The remaining ∼75 per cent of main-sequence binaries are wide enough to avoid mass transfer interactions. In these cases the more massive stars evolve like single stars until they eventually become white dwarfs. The orbital separations of such WDMS binaries are similar to those of the main-sequence binaries from which they descend.

During the last years we have mined the Sloan Digital Sky Survey (SDSS; York et al. 2000) spectroscopic data base to build up the largest, most homogeneous and complete catalogue of WDMS binaries (Rebassa-Mansergas et al. 2010, 2012a, 2013b), which contains 2316 systems as for data release (DR) 8. Observational studies led by our team have resulted in the identification of 1050 wide SDSS WDMS binaries and 206 PCEBs (Rebassa-Mansergas et al.

★ E-mail: alberto.rebassa@upc.edu

2007; Schreiber et al. 2008, 2010; Rebassa-Mansergas et al. 2011), for which we have measured the orbital period of 90 (Rebassa-Mansergas et al. 2008; Nebot Gómez-Morán et al. 2011; Rebassa-Mansergas et al. 2012b).

The analysis of the entire SDSS WDMS binary sample, as well as the sub-samples of close PCEBs and widely separated WDMS binaries have led to numerous advances in several fields of modern astrophysics. These include for example: constraining current theories of close compact binary evolution (Davis, Kolb & Willems 2010; Zorotovic et al. 2010, 2011a; Rebassa-Mansergas et al. 2012b); demonstrating in a robust way that the majority of low-mass white dwarfs are formed in binaries (Rebassa-Mansergas et al. 2011); constraining the pairing properties of main-sequence stars (Ferrario 2012); providing robust observational evidence for disrupted magnetic braking (Schreiber et al. 2010); constraining the rotation-age-activity relation of low-mass main-sequence stars (Rebassa-Mansergas, Schreiber & Gänsicke 2013a); studying the statistical properties of the PCEB population using Monte Carlo techniques (Toonen & Nelemans 2013; Camacho et al. 2014; Zorotovic et al. 2014); analysing why the average mass of white dwarfs in cataclysmic variables is significantly larger than the average mass of single white dwarfs (Zorotovic, Schreiber & Gänsicke 2011b; Nelemans et al. 2016; Schreiber, Zorotovic & Wijnen 2016); testing hierarchical probabilistic models used to infer properties of unseen companions to low-mass white dwarfs (Andrews, Price-Whelan & Agüeros 2014); detecting new gravitational wave verification sources (Kilic et al. 2014); analysing the interior structural effects of common envelope evolution on low-mass pulsating white dwarfs (Hermes et al. 2015). In addition, many eclipsing SDSS PCEBs have been identified (Nebot Gómez-Morán et al. 2009; Pyrzas et al. 2009, 2012; Parsons et al. 2013, 2015) which are being used to test theoretical mass–radius relations of both white dwarfs and low-mass main-sequence stars (Parsons et al. 2012b,a), as well as the existence of circumbinary planets (Zorotovic & Schreiber 2013; Marsh et al. 2014; Parsons et al. 2014).

The motivation of this paper is to update our spectroscopic catalogue of SDSS WDMS binaries by searching for new identifications within the third survey generation of the SDSS (SDSS III; Eisenstein et al. 2011) to thus increase the number of systems available for follow-up studies.[1]

2 THE SDSS III SURVEY

In this work, we search for WDMS binaries within the spectroscopic data base of the SDSS III, i.e. the ninth (SDSS-III Collaboration et al. 2014), tenth (Ahn et al. 2014), eleventh and twelfth (Alam et al. 2015) DRs of the SDSS. In particular, we mined the optical ($R \sim 2000$) spectra obtained by the Sloan Exploration of Galactic Understanding and Evolution 2 survey (SEGUE-2; Rockosi et al., in preparation) and the Baryon Oscillation Spectroscopic Survey (BOSS; Dawson et al. 2013).

BOSS uses a new set of spectrographs with 1000 fibres available per exposure. The main goal of the survey is to obtain spectra for galaxies and quasars selected from the SDSS imaging data to study the baryon oscillation feature in the clustering of galaxies and Lyman α absorption along the line of sight to distant quasars.

BOSS uses a different target selection criteria for targeting quasars (Ross et al. 2012) than the one employed by the SDSS I/II surveys. Thus, whilst SDSS I/II targeted objects with $i < 19.1$, BOSS went down to $g < 22.0$ in order to give a significantly higher surface density of targets than in SDSS I/II (Ross et al. 2012). BOSS has obtained a total number of 457 1520 spectra. Because WDMS binaries and quasars overlap in colour space (Smolčić et al. 2004), we expect a large number of WDMS binaries being (most likely accidentally) observed by the BOSS survey. SEGUE-2 used the SDSS I/II spectrographs to obtain spectra of stars at high and low Galactic latitudes to study Galactic structure, dynamics and stellar populations. SEGUE-2 gathered a total of 155 520 spectra.

3 IDENTIFICATION OF WDMS BINARIES

In Rebassa-Mansergas et al. (2010), we developed a routine based on reduced χ^2 and signal-to-noise (SN) ratio constraints (χ^2-SN method hereafter) to identify spectroscopic SDSS WDMS binaries. As in our previous works, we use this method here for identifying WDMS binaries observed by the SDSS III survey.

In a first step, we χ^2-fit all SDSS III spectra with a grid of 163 WDMS binary templates covering a wide range of white dwarf effective temperatures (6000–100 000 K) and surface gravities (6.5–9.5 dex), and secondary star M-dwarf spectral types (M0–M9)[2] and represent the reduced χ^2 values as a function of SN ratio for each template. We then define an equation of the form

$$\chi^2_{\max} = a \times SN^b, \tag{1}$$

and consider as WDMS binary candidates all objects below this curve ($\chi^2_{\mathrm{spec}} < \chi^2_{\max}$), where a and b are free parameters defined for each template and χ^2_{spec} is the χ^2 that results from fitting a considered spectrum with a given template (see Rebassa-Mansergas et al. 2010 for a complete description of the method). The form of equation (1) is defined to account for systematic errors between template and observed spectra, which become more important the larger the SN ratio is. This exercise resulted in 9593 WDMS binary candidate spectra which were visually inspected. We also inspected their SDSS images for morphological problems and made use of the *GALEX* ultraviolet (Martin et al. 2005; Morrissey et al. 2005) and UKIDSS infrared (Dye et al. 2006; Hewett et al. 2006; Lawrence et al. 2007) magnitudes to probe for the presence of excess flux at the blue and red ends of the SDSS spectra, respectively.

We found 872 of the 9593 selected spectra to be genuine WDMS binaries and we considered 47 spectra as WDMS binary candidates. In what follows, we flag an object to be a WDMS binary candidate when the spectrum is that of a white dwarf (main-sequence star) displaying some red (blue) flux excess which cannot be confirmed to arise from a companion due to the lack of *GALEX* (UKIDSS) magnitudes.

The above outlined χ^2-SN method has been proven to be very efficient at identifying WDMS binaries, achieving a completeness (defined as the ratio between the number of SDSS WDMS binary spectra we have successfully identified and the total number of SDSS WDMS binary spectra observed) around 96 per cent (Rebassa-Mansergas et al. 2010, 2012a, 2013b). However, it is important to keep in mind that the limiting magnitude of the quasar survey has been modified from $i < 19.1$ in SDSS I/II to $g < 22$ in SDSS III. We therefore expect a considerable fraction of SDSS III

---

[1] The SDSS DR 8 contains the first set of spectra observed by SDSS III, which are not considered here because we have already identified WDMS binaries within this DR. Thus, in this paper we will consider SDSS III as all data collected from DR 9 to DR 12.

[2] Due to selection effects the vast majority of SDSS WDMS binaries contain a low-mass M-dwarf companion, see Rebassa-Mansergas et al. (2010).

WDMS binary spectra to generally be of lower SN ratio than those from SDSS I/II. Low SN ratio spectra ($\lesssim 5$) are challenging to classify for any method, including our χ^2-SN routine.

Ren et al. (2014) developed an independent strategy based on the wavelet transform (WT; e.g. Chui 1992) that proved to be efficient at identifying such low SN ratio WDMS binary spectra. Ren et al. (2014) searched for WDMS binaries among spectra obtained as part of the LAMOST (Large Aperture Multi-Object Spectroscopy Telescope) surveys (Cui et al. 2012; Luo et al. 2012; Liu et al. 2014; Yuan et al. 2015a). The analysis unit of the WT is the local flux of the spectrum, i.e. the selected spectral features. Thus, for a given spectrum, the WT recognizes the spectral features rather than the global continuum. The WT decomposes the considered features of a given spectrum into approximation signals, also referred to as approximation coefficients. The wavelength values under the considered spectral regions where the WT is applied are converted into 'data points'. The outcome of a WT can be considered, for comparative purposes, as a smooth version of the spectrum. The WT is therefore a suitable method to identify spectral features among low-SN ratio spectra, and we adopt it here to complement our search of SDSS III WDMS binaries.

We applied the WT to the following spectral regions: the 3910–4422 Å range thus covering the Balmer lines typical of hydrogen-rich (DA) white dwarfs, and the 6800–8496 Å range which samples a large number of TiO and VO molecular bands typical of low-mass main-sequence stars. This choice implies that our WT routine is most efficient at identifying WDMS binaries containing DA white dwarfs, by far the most common among white dwarfs. Once we applied the WT to all SDSS III spectra, WDMS binaries could be easily selected by applying a number of cuts to the approximation coefficients and data points obtained for each spectrum (see equations 1 and 2 of Ren et al. 2014). Applying the WT and aforementioned cuts to all SDSS III spectra resulted in 36 543 selected spectra. We visually inspected the spectra and found 1072 of these to be genuine WDMS binaries, and 30 to be WDMS binary candidates.

4 THE SDSS SPECTROSCOPIC CATALOGUE OF WDMS BINARIES

Here we quantify the total number of SDSS III WDMS binary spectra we identified in the previous section and determine how many of these objects are new additions to our latest SDSS DR 8 WDMS binary catalogue. We also estimate the completeness of our SDSS III WDMS binary sample and compare our catalogue to previously published lists of SDSS III WDMS binaries. Finally, we provide the total number of systems that form the spectroscopic catalogue of SDSS WDMS binaries.

4.1 The SDSS III WDMS binary sample

As explained above, 872 and 47 SDSS III WDMS binary and candidate spectra, respectively, have been identified following the χ^2-SN ratio method. Also, 1072 and 30 WDMS binary and candidate spectra were identified following the WT method (see Table 1). Whilst 670 (10 candidates) are systems commonly identified by both methods, 202 (37 candidates) and 402 (20 candidates) are independently found by the χ^2-SN ratio and the WT routines, respectively (see Fig. 1, top panel). This brings the total number of SDSS III WDMS binary and candidate spectra we have identified to 1274 and 67, respectively (Table 1).

Inspection of the numbers outlined above reveals that the χ^2-SN ratio method has identified only ~68 per cent of our total number

Table 1. Number of WDMS binary spectra we have identified or studied (first column), number of WDMS binary spectra added to the SDSS III sample identified in this work (second column) and total number of SDSS III WDMS binary spectra. In brackets we give the number of WDMS binary candidate spectra.

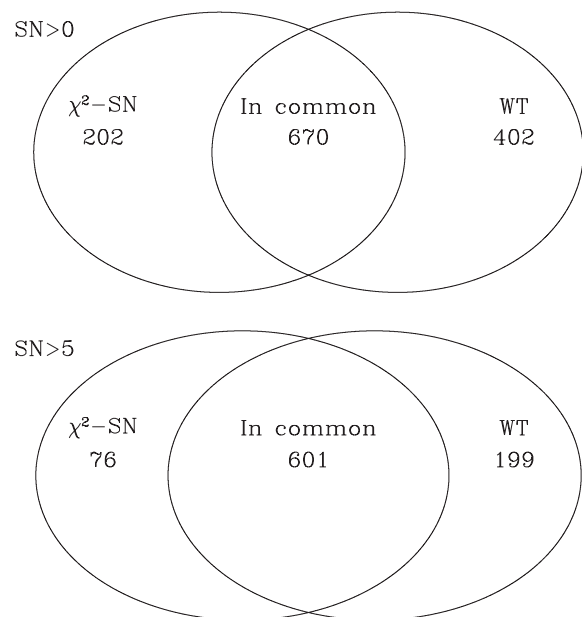| Exercise	$N_{\rm sample}$	$N_{\rm added}$	$N_{\rm SDSS\,III}$
χ^2-SN	872(47)	–	872(47)
WT	1072(30)	402(20)	1274(67)
Completeness	933(26)	30(4)	1304(71)
Li et al. (2014)	152(4)	5(3)	1309(74)
Kepler et al. (2015)	158(6)	5(4)	1314(78)
Kepler et al. (2016)	127(2)	5(1)	1319(79)
Gentile Fusillo, Gänsicke & Greiss (2015)	93(0)	2(0)	1321(79)
WT to SDSS I/II	1852(13)	46(12)	–
Total in this work			1367(91)

Figure 1. Top panel: Venn diagram for WDMS binaries identified by the χ^2-SN (left) and WT (right) methods. Bottom panel: the same but considering only spectra of SN > 5.

of SDSS III WDMS binary spectra and that the WT method has successfully identified ~84 per cent of the total number. That is, the WDMS binary samples identified by the χ^2-SN and the WT methods are ~68 and ~84 per cent complete, respectively (the completeness of the overall sample is derived in the next section). Whilst the ~84 per cent of WDMS binary spectra found by the WT method is in agreement with the results of Ren et al. (2014) – they estimate a completeness of ~90 per cent – the ~68 per cent of WDMS binary spectra identified by the χ^2-SN ratio method is considerably lower than the ~96 per cent determined in our previous works (Rebassa-Mansergas et al. 2010, 2012a, 2013b). As we show in Fig. 2, this seems to be simply a consequence of SDSS III WDMS binary spectra being generally of lower SN ratio due to the limiting magnitude of the BOSS quasar survey (Ross et al. 2012). Indeed, we investigated the 402 WDMS binary spectra the χ^2-SN ratio method failed to identify and found that 81 per cent of them are of SN ≤ 5. If we consider only WDMS binary spectra of SN ratio above 5, i.e. a total of 876 spectra, then the χ^2-SN and WT methods successfully identify 800 and 677 spectra, respectively, 601 in common (see
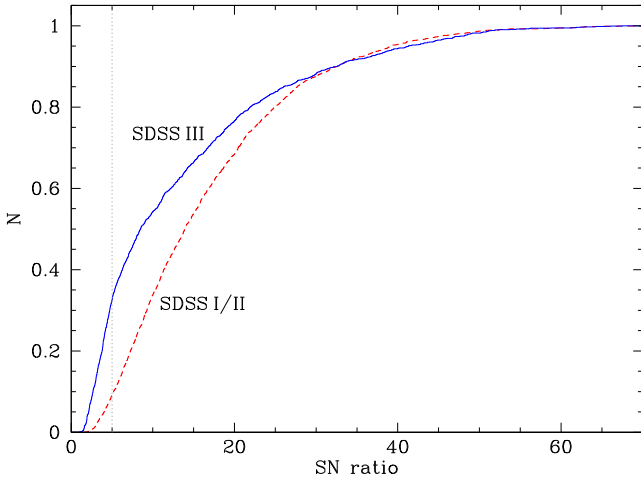
Figure 2. Cumulative distributions of SN ratio of WDMS binary spectra identified within SDSS I/II (red dashed line) and SDSS III (blue solid line). The grey vertical line indicates SN = 5. SDSS III contains a considerably larger fraction of low ($\leq$5) SN spectra.
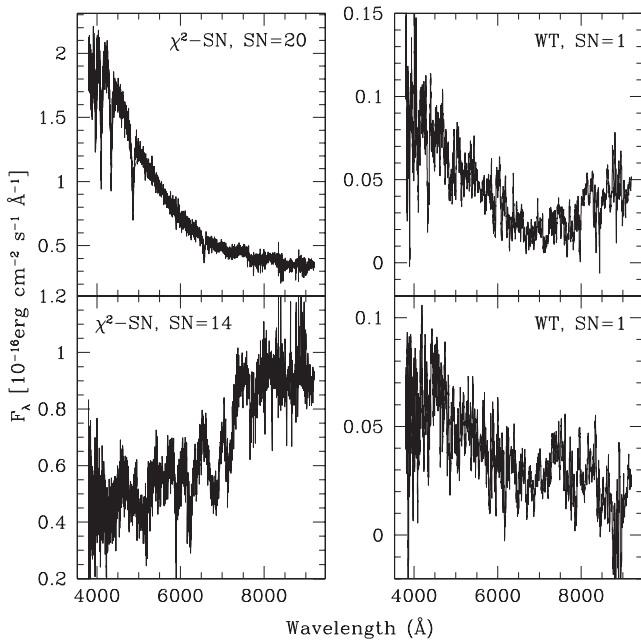

Figure 3. Example WDMS binary spectra found only by the χ^2-SN method (left-hand panels) and only by the WT method (right-hand panels). The spectra in the right-hand panels have been smoothed using a filter size of 15 due to the very low SN ratio. Whilst the χ^2-SN method is more efficient at finding WDMS binaries in which one of the two components dominates the spectrum, the WT method is more efficient at finding low SN ratio WDMS binary spectra.

Fig. 1, bottom panel). That is, $\sim$91 and $\sim$77 per cent of the total number of WDMS binary spectra with SN ratio >5. This implies the WT method is considerably more efficient at identifying WDMS binary spectra of low SN ratio. We also visually inspected the list of spectra the WT methods failed to identify and found that it mostly contained WDMS binaries in which the flux of one of the two components dominates the spectrum. Therefore, we conclude that the χ^2-SN ratio and WT methods efficiently complement each other for identifying WDMS binaries within SDSS III. In Fig. 3, we show a few examples of WDMS binary spectra identified only by the
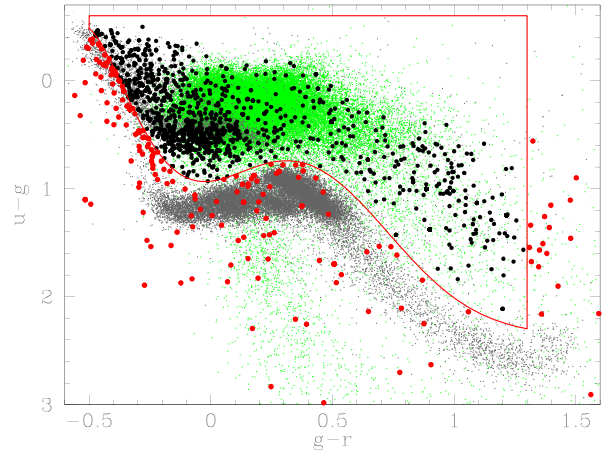

Figure 4. SDSS III WDMS binaries identified by the χ^2-SN and WT methods (black solid dots), main-sequence stars (grey dots) and quasars (green solid dots) in the $u - g$ versus $g - r$ colour plane. Colour cuts for WDMS binaries are given as solid red lines. $\sim$15 per cent of all WDMS binaries fall outside the colour selection mainly due to the large photometric uncertainties.

χ^2-SN ratio method and only by the WT method. In the following section, we analyse the completeness of the entire SDSS III WDMS binary sample.

4.2 Completeness of the SDSS III WDMS binary sample

Using the χ^2-SN and WT methods we have identified a total of 1274 and 67 SDSS III WDMS binary and candidate spectra (Table 1). Here, we analyse how complete this sample is.

WDMS binaries define a clear region in the $u - g$ versus $g - r$ colour–colour diagram (Smolčić et al. 2004) and can be selected via the colour cuts provided by Rebassa-Mansergas et al. (2013b, see also Fig. 4):

$$
\begin{aligned}
(u - g) < &\; 0.93 - 0.27 \times (g - r) - 4.7 \times (g - r)^2 \\
&+ 12.38 \times (g - r)^3 + 3.08 \times (g - r)^4 \\
&- 22.19 \times (g - r)^5 + 16.67 \times (g - r)^6 \\
&- 3.89 \times (g - r)^7,
\end{aligned}
\tag{2}
$$

$$
(u - g) > -0.6,
\tag{3}
$$

$$
-0.5 < (g - r) < 1.3.
\tag{4}
$$

Obviously, the efficiency of the above colour cuts in selecting WDMS binaries relies on the accuracy of the SDSS photometry. This is difficult to achieve in cases where the two components are partially resolved (blended) in the SDSS images, when the systems are too faint so that their magnitudes are associated with large uncertainties, and/or when one of the two stars outshines its companion. This results in $\sim$15 per cent of the SDSS III WDMS binaries identified by the χ^2-SN and WT methods to fall outside the colour cuts (see Fig. 4). However, it has to be stressed that the colour selection can be used to test the completeness of our spectroscopic sample, as visual inspection of all sources with available SDSS spectra satisfying the cuts would result in a WDMS binary sample that is 100 per cent complete (within the colour selection). We hence used the *casjobs* interface to select all spectroscopic point sources with clean photometry satisfying the cuts. This resulted in 126 4475 objects among 712 1388 photometric sources. Excluding all targets with spectroscopic redshifs below 0.05 (to thus avoid quasar

Table 2. Combination of WDMS binary stellar parameters and flux ratios that allow the detection of the two stellar components in the SDSS spectrum. The flux ratios are directly derived from the effective temperatures of the two components. The effective temperatures of the secondary stars are obtained using the empirical spectral type-effective temperature relation of Camacho et al. (2014).

log $(g)_{WD}$ (dex)	Sp_{sec}	$T_{eff,sec}$ (K)	$T_{eff,WD}$ (K)	Flux ratio	log $(g)_{WD}$ (dex)	Sp_{sec}	$T_{eff,sec}$ (K)	$T_{eff,WD}$ (K)	Flux ratio
6.5	0	4044	9000–100000	4.08×10^{-2}–2.67×10^{-6}	8.0	5	3063	6000–100000	6.79×10^{-2}–8.80×10^{-7}
6.5	1	3738	8000–100000	4.77×10^{-2}–1.95×10^{-6}	8.0	6	2947	6000–100000	5.82×10^{-2}–7.54×10^{-7}
6.5	2	3505	7000–100000	6.29×10^{-2}–1.51×10^{-6}	8.0	7	2817	6000–70000	4.86×10^{-2}–2.62×10^{-6}
6.5	3	3325	6000–100000	9.43×10^{-2}–1.22×10^{-6}	8.0	8	2658	6000–20000	3.85×10^{-2}–3.12×10^{-4}
6.5	4	3184	6000–100000	7.93×10^{-2}–1.03×10^{-6}	8.0	9	2453	6000–13000	2.79×10^{-2}–1.27×10^{-3}
6.5	5	3063	6000–75000	6.79×10^{-2}–2.78×10^{-6}	8.5	0	4044	20000–100000	1.67×10^{-3}–2.67×10^{-6}
6.5	6	2947	6000–30000	5.82×10^{-2}–9.31×10^{-5}	8.5	1	3738	14000–100000	5.08×10^{-3}–1.95×10^{-6}
6.5	7	2903	6000–18000	5.48×10^{-2}–6.00×10^{-4}	8.5	2	3505	11000–100000	1.03×10^{-2}–1.51×10^{-6}
6.5	8	2658	6000–9000	3.85×10^{-2}–7.61×10^{-3}	8.5	3	3325	9000–100000	1.86×10^{-2}–1.22×10^{-6}
6.5	9	2453	6000–7000	2.79×10^{-2}–1.51×10^{-2}	8.5	4	3184	8000–100000	2.51×10^{-2}–1.03×10^{-6}
7.0	0	4044	9000–100000	4.08×10^{-2}–2.67×10^{-6}	8.5	5	3063	7000–100000	3.67×10^{-2}–8.80×10^{-7}
7.0	1	3738	8000–100000	4.77×10^{-2}–1.95×10^{-6}	8.5	6	2947	6000–100000	5.82×10^{-2}–7.54×10^{-7}
7.0	2	3505	7000–100000	6.29×10^{-2}–1.51×10^{-6}	8.5	7	2817	6000–100000	4.86×10^{-2}–6.30×10^{-7}
7.0	3	3325	6000–100000	9.43×10^{-2}–1.22×10^{-6}	8.5	8	2658	6000–36000	3.85×10^{-2}–2.97×10^{-5}
7.0	4	3184	6000–100000	7.93×10^{-2}–1.03×10^{-6}	8.5	9	2453	6000–20000	2.79×10^{-2}–2.26×10^{-4}
7.0	5	3063	6000–100000	6.79×10^{-2}–8.80×10^{-7}	9.0	0	4044	30000–100000	3.30×10^{-4}–2.67×10^{-6}
7.0	6	2947	6000–55000	5.82×10^{-2}–8.24×10^{-6}	9.0	1	3738	24000–100000	5.88×10^{-4}–1.95×10^{-6}
7.0	7	2817	6000–24000	4.86×10^{-2}–1.90×10^{-4}	9.0	2	3505	18000–100000	1.44×10^{-3}–1.51×10^{-6}
7.0	8	2658	6000–10000	3.85×10^{-2}–4.99×10^{-3}	9.0	3	3325	12000–100000	5.89×10^{-3}–1.22×10^{-6}
7.0	9	2453	6000–8000	2.79×10^{-2}–8.84×10^{-3}	9.0	4	3184	10000–100000	1.03×10^{-2}–1.03×10^{-6}
7.5	0	4044	11000–100000	1.83×10^{-2}–2.67×10^{-6}	9.0	5	3063	9000–100000	1.34×10^{-2}–8.80×10^{-7}
7.5	1	3738	9000–100000	2.98×10^{-2}–1.95×10^{-6}	9.0	6	2947	7000–100000	3.14×10^{-2}–7.54×10^{-7}
7.5	2	3505	8000–100000	3.68×10^{-2}–1.51×10^{-6}	9.0	7	2817	6000–100000	4.86×10^{-2}–6.30×10^{-7}
7.5	3	3325	7000–100000	5.09×10^{-2}–1.22×10^{-6}	9.0	8	2658	6000–95000	3.85×10^{-2}–6.13×10^{-7}
7.5	4	3184	6000–100000	7.93×10^{-2}–1.03×10^{-6}	9.0	9	2453	6000–30000	2.79×10^{-2}–4.47×10^{-5}
7.5	5	3063	6000–100000	6.79×10^{-2}–8.80×10^{-7}	9.5	1	3738	60000–100000	1.51×10^{-5}–1.95×10^{-6}
7.5	6	2947	6000–95000	5.82×10^{-2}–9.26×10^{-7}	9.5	2	3505	30000–100000	1.86×10^{-4}–1.51×10^{-6}
7.5	7	2817	6000–40000	4.86×10^{-2}–2.46×10^{-5}	9.5	3	3325	22000–100000	5.22×10^{-4}–1.22×10^{-6}
7.5	8	2658	6000–16000	3.85×10^{-2}–7.62×10^{-4}	9.5	4	3184	18000–100000	9.79×10^{-4}–1.03×10^{-6}
7.5	9	2453	6000–10000	2.79×10^{-2}–3.62×10^{-3}	9.5	5	3063	14000–100000	2.29×10^{-3}–8.80×10^{-7}
8.0	0	4044	15000–100000	5.28×10^{-3}–2.67×10^{-6}	9.5	6	2947	10000–100000	7.54×10^{-3}–7.54×10^{-7}
8.0	1	3738	11000–100000	1.33×10^{-2}–1.95×10^{-6}	9.5	7	2817	8000–100000	1.54×10^{-2}–6.30×10^{-7}
8.0	2	3505	9000–100000	2.30×10^{-2}–1.51×10^{-6}	9.5	8	2658	7000–100000	2.08×10^{-2}–1.51×10^{-2}
8.0	3	3325	8000–100000	2.98×10^{-2}–1.22×10^{-6}	9.5	9	2453	10000–100000	3.62×10^{-3}–3.62×10^{-7}
8.0	4	3184	7000–100000	4.28×10^{-2}–1.03×10^{-6}					

contamination) we ended up with 50 691 SDSS III selected objects (in this exercise we did not take into account all spectra contained in the DR 8 or earlier SDSS releases). We visually inspected the spectra and identified 933 (26) WDMS binary (candidate) spectra (Table 1). Of these, only 30 (4) spectra were not included in our list of systems identified by the χ^2-SN and WT methods. Visual inspection of the spectra we failed to identify revealed that, in most of the cases, one of the two binary components dominates the spectral energy distribution. This exercise strongly suggests that our SDSS III WDMS binary sample is highly complete ($\simeq$96 per cent) and that the WDMS binary spectra we miss are likely dominated by the flux of one of the binary components. We include the 34 missed spectra in our sample and thus increase the number of SDSS III WDMS binary and candidate spectra to 1304 and 71, respectively (Table 1).

It is important to emphasize that, although our spectroscopic sample is highly complete, the population of SDSS WDMS binaries does not represent the real and unbiased population of WDMS binaries. First, there exists an intrinsic binary bias that allows us to detect only those objects displaying both components in the SDSS spectra. We studied this issue in detail in Camacho et al. (2014) so we here provide in Table 2 the combination of stellar parameters and flux ratios that allow the detection of the two components in the SDSS spectra. Secondly, the majority of SDSS WDMS binaries have been observed simply because they have similar colours to those of quasars. This effect is clearly visible in Fig. 4, where there is a clear scarcity of WDMS systems with $g - r > 0.5$ colours, and also in Fig. 5 (top panel), where we show a density map illustrating the fraction of SDSS objects with available spectra. This implies the majority of spectroscopic SDSS WDMS binaries generally contain hot white dwarfs (see further details in Section 6).

4.3 Comparison with Li et al. (2014)

Li et al. (2014) provided a list of 227 DR 9 WDMS binaries, of which 148 (1) are included in our WDMS binary (candidate) list. Of the remaining 78, 70 spectra are not considered as WDMS binaries by us (the majority are main sequence plus main-sequence superpositions and also some single white dwarfs), and 5 (3) are WDMS binary (candidate) spectra that we missed. This implies we have successfully identified ~95 per cent of the total WDMS binary sample of Li et al. (2014). The missed spectra are dominated by the flux emission of one of the two components and we include them
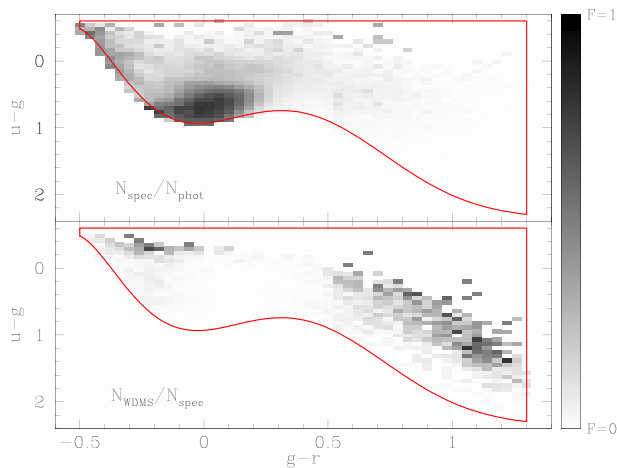
Figure 5. Top panel: density map illustrating the fraction of SDSS objects with available spectroscopy ($F = N_{spec}/N_{phot}$, ranging from 0 to 1, where N_{spec} and N_{phot} are the number of SDSS objects with available spectra and the number of SDSS photometric point sources, respectively). As expected, the fraction is the highest in quasar dominated areas. Bottom panel: density map illustrating the fraction of WDMS binaries among objects with available spectroscopy ($F = N_{WDMS}/N_{spec}$, ranging from 0 to 1, where N_{WDMS} is the number of SDSS WDMS binaries). The fraction is the lowest in quasar dominated areas due to the large number of observed quasars.

in our lists, thus raising the number of SDSS III WDMS binary and candidate spectra to 1309 and 74, respectively (Table 1). We also note that our list contains 447 WDMS binary spectra that are part of SDSS DR 9 which are not included in the catalogue of Li et al. (2014). This indicates that our routines are much more efficient at identifying SDSS WDMS binaries, and that the catalogue of SDSS WDMS binaries by Li et al. (2014) is highly incomplete.

Li et al. (2014) provide effective temperatures, surface gravities and masses for the white dwarfs in their WDMS binary sample. As we also do, they derive these parameters fitting the white dwarf spectra with the 1D white dwarf model grid of Koester (2010). However, they do not apply 3D corrections to avoid the so-called log *g* problem at low effective temperatures (see further details in Section 5).

4.4 Comparison with Kepler et al. (2015) and Kepler et al. (2016)

An additional list of 177 DR 9–10 SDSS WDMS binary spectra has been provided by Kepler et al. (2015). 153 (2) of these are included in our WDMS binary (candidate) list, we only missed 5 (4) WDMS binary (candidate) spectra (Table 1), the majority dominated by the flux contribution of the white dwarf. We classify the remaining 13 spectra as single white dwarfs or main sequence plus main-sequence superpositions. Hence, we have successfully identified ∼94 per cent of the total sample provided by Kepler et al. (2015). We include the nine missed objects in our lists and increase to 1314 and 78 the number of WDMS binary and candidate spectra, respectively (Table 1). Moreover, we note that we have identified 759 DR 9–10 WDMS binary spectra that are not included in the list of Kepler et al. (2015). The fact that Kepler et al. (2015) missed this large number of WDMS binary spectra is not too surprising, as their main focus was to identify single white dwarfs.

Kepler et al. (2016) presented an updated SDSS white dwarf catalogue from DR 12, which includes 160 new WDMS binary

spectra. 123 of these are included in our lists, 122 as genuine WDMS binaries and 1 as a candidate (Table 1). The remaining 37 spectra include 5 (1) WDMS binaries (candidate) that we missed and 31 objects that we classify as either single white dwarfs, cataclysmic variables or unclassified. Thus, we have identified ∼95 per cent of WDMS binary sample provided by Kepler et al. (2016). We include the six missed objects in our lists thus increasing to 1319 and 79 the number of WDMS binary and candidate spectra, respectively (Table 1). We also note that our catalogue contains 337 DR 12 WDMS binary spectra that Kepler et al. (2016) did not identify.

4.5 Comparison with Gentile Fusillo et al. (2015)

Gentile Fusillo et al. (2015) developed a method which uses cuts in colour–colour and reduced proper motion-colour space to select ∼23 000 high-fidelity white dwarf candidates. Among the 8701 of them with available spectra, they classified 98 as WDMS binaries, of which 91 are included in our WDMS binary catalogue. The remaining seven include two WDMS binaries that we missed clearly dominated by the flux contribution of the white dwarfs and five objects that we classify as single white dwarfs or cataclysmic variables. We thus have identified 99 per cent of the WDMS binary sample of Gentile Fusillo et al. (2015). We include the two missed objects in our list and thus raise to 1321 and 79 the number of WDMS binary and candidate spectra, respectively (Table 1).

4.6 Applying the WT method to DR 8 spectra

We have shown that the WT is more efficient than the χ^2-SN method at identifying SDSS WDMS binaries of low SN ratio spectra (Section 3). It is therefore plausible that Rebassa-Mansergas et al. (2010, 2012a, 2013b) missed a fraction of low SN ratio SDSS I/II WDMS binary spectra. In order to investigate this we applied the WT as specified in Section 3 to all SDSS DR 8 spectra, which resulted in 20 060 selected candidates. We found 1852 to be genuine WDMS binaries and 13 are considered as WDMS binary candidates. Only the 12 candidate spectra and 46 WDMS binary spectra are not included in our SDSS WDMS binary catalogue (Table 1) – ∼3 per cent of the total identified sample (Rebassa-Mansergas et al. 2013b).

4.7 The final number of spectroscopic SDSS WDMS binaries

In the previous sections, we have identified a total of 1367 (91) WDMS binary (candidate) spectra (Table 1). We cross-correlate this list with our latest catalogue of 2316 DR 8 WDMS binaries (Rebassa-Mansergas et al. 2013b) and find 979 new systems, 647 of which have not been published before (Table 3). Thus, the total number of spectroscopic SDSS WDMS binaries raises to 3295, i.e. an increase of ∼40 per cent. We have updated our web site http://www.sdss-wdms.org including the new systems and spectra identified in this work. The object names, coordinates and *ugriz* magnitudes of the SDSS WDMS binaries found in this work are also available in the electronic edition of the paper.

5 STELLAR PARAMETERS

We here derive white dwarf effective temperatures, surface gravities and masses, and secondary star spectral types for all WDMS binaries identified in this work. To that end we use the decomposition/fitting routine outlined by Rebassa-Mansergas et al. (2007). We first use a combined set of observed M dwarf and white dwarf templates to

Table 3. Number of SDSS WDMS binary spectra identified in this work ($N_{spectra}$), number of unique sources after excluding duplicated spectra (N_{unique}), number of additions to our latest DR 8 spectroscopic catalogue after excluding systems that were already observed ($N_{additions}$), total number of spectroscopic SDSS DR 12 WDMS binaries (N_{total}) and number of new systems that have not been published before (N_{new}). In brackets we give the number of WDMS binary candidates.

$N_{spectra}$	1367 (91)
N_{unique}	1177 (91)
$N_{additions}$	892 (87)
N_{total}	3115 (180)
N_{new}	572 (75)

fit a given SDSS WDMS binary spectrum and record the spectral type of the secondary star. We then subtract the best-fitting M dwarf template and fit the normalized Balmer lines of the residual white dwarf spectrum with a model grid of DA white dwarfs (Koester 2010) to derive the effective temperature and surface gravity. The Balmer line fitting is subject to a 'cold/hot' solution degeneracy, which is broken fitting the entire spectrum (continuum plus lines) with the same grid of model spectra (note that the continuum is most sensitive to the effective temperature). Given that 1D white dwarf model spectra such as those used in this work yield overestimated surface gravity values for white dwarfs of effective temperatures below ∼12 000 K (e.g. Koester et al. 2009; Tremblay et al. 2011), we apply the 3D corrections of Tremblay et al. (2013) to our effective temperature and surface gravity determinations (we apply

the 3D corrections to all SDSS WDMS binaries we identified in previous works too, as these corrections were not available at that time). We then interpolate these values in the updated cooling sequences of Bergeron, Wesemael & Beauchamp (1995) and derive white dwarf masses. For the sake of comparison, we also derive the white dwarf masses using the models of Renedo et al. (2010) and find no substantial difference between the values obtained from the two cooling sequences. The SDSS spectra of the WDMS binaries for which we cannot obtain stellar parameters are either too noisy and/or are dominated by the flux from one of the two stellar components. In cases where more than one spectrum per target is available we average the corresponding parameter values. The white dwarf effective temperatures, surface gravities and masses, and secondary star spectral types that result from fitting spectra of the same targets are found to agree at the 1.5σ level in 53, 64, 67 and 89 per cent of the cases, respectively. The stellar parameters are accessible via our web site http://www.sdss-wdms.org.

The parameter distributions are shown in Fig. 6, where we divide the sample into BOSS (top panels) and SEGUE-2 (second top panels) WDMS binaries. In the distributions we only consider white dwarf effective temperatures with a relative error under 10 per cent, and white dwarf surface gravities and masses of absolute errors under 0.075 $M_\odot$ and 0.075 dex, respectively. For completeness, in the mid-bottom panels of the same figure we also provide the parameter distributions of SDSS I/II WDMS binaries, where these are divided into objects that were observed by the Legacy (Adelman-McCarthy et al. 2008; Abazajian et al. 2009) survey of quasars and galaxies (hereafter Legacy WDMS binaries) and objects that were observed as part of our dedicated SEGUE (the SDSS Extension for Galactic Understanding and Exploration; Yanny et al. 2009)
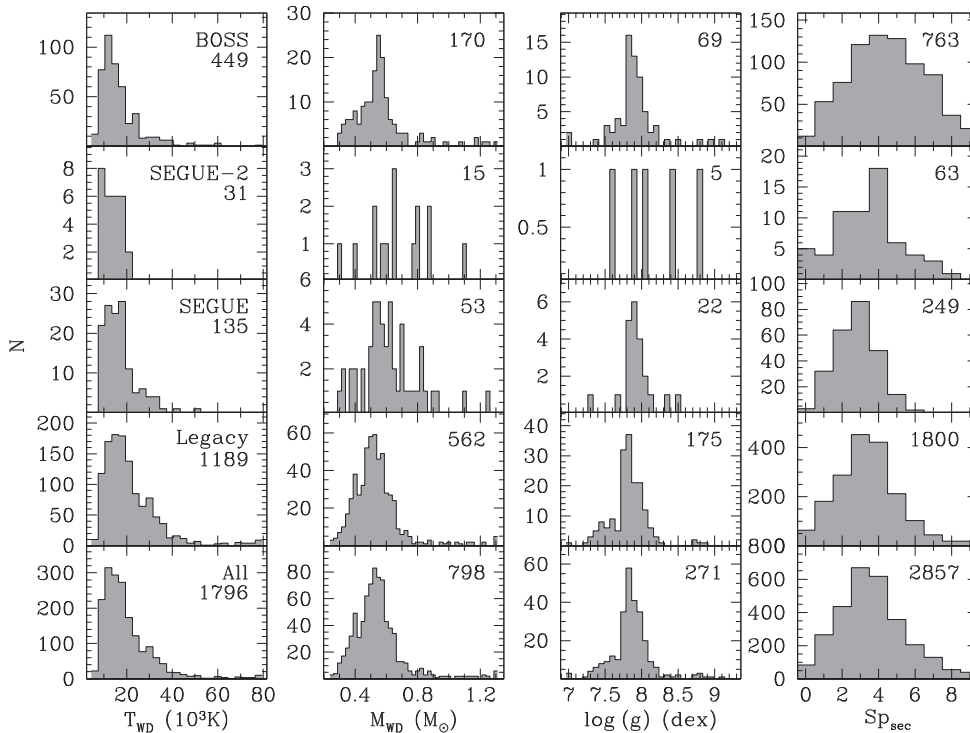

Figure 6. From left to right the distribution of white dwarf effective temperatures, masses, surface gravities and secondary star (M) spectral types for the WDMS binaries observed by the BOSS, SEGUE-2, SEGUE and Legacy surveys of SDSS. Given that WDMS binaries can be observed by more than one survey, we consider them to be part of as many samples as different surveys have observed them. In the bottom panels, we provide the distributions for the entire (All) spectroscopic catalogue of SDSS DR 12 WDMS binaries. In this case WDMS binaries that are observed by more than one survey are only considered once. We also provide the number of systems per distribution in each panel.
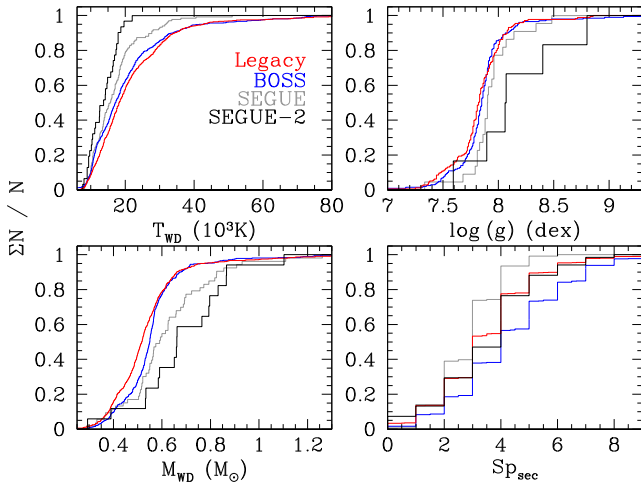
Figure 7. Cumulative distributions of white dwarf effective temperature (top left), mass (bottom left), surface gravity (top right) and secondary star spectral type (bottom right) for the BOSS, SEGUE-2, Legacy and SEGUE WDMS binary populations.

Table 4. KS and χ^2 probabilities that result from comparing the cumulative distributions (Fig. 7) of the different SDSS WDMS binary populations.

T_{WD}	SEGUE-2	SEGUE	Legacy
BOSS	4×10^{-4}	3×10^{-3}	3×10^{-4}
SEGUE-2		0.06	2×10^{-5}
SEGUE			2×10^{-5}
M_{WD}	SEGUE-2	SEGUE	Legacy
BOSS	2×10^{-4}	3×10^{-3}	9×10^{-7}
SEGUE-2		0.19	1×10^{-4}
SEGUE			2×10^{-4}
$\log g$	SEGUE-2	SEGUE	Legacy
BOSS	0.03	0.05	0.11
SEGUE-2		0.15	0.03
SEGUE			0.02
Sp	SEGUE-2	SEGUE	Legacy
BOSS	0.01	0	0
SEGUE-2		0	0.55
SEGUE			0

survey for targeting objects containing cool white dwarfs and early-type companions (Rebassa-Mansergas et al. 2012a). We restrict the Legacy and SEGUE samples by the same error parameter cuts as above outlined. It is also important to mention that we do not exclude duplicated targets that have been observed by different surveys. Thus, for example, a given WDMS binary is part of both the SEGUE and BOSS populations if it has been independently observed by both surveys. Finally, in the bottom panel of Fig. 6 we provide the parameter distributions of the entire spectroscopic catalogue of SDSS DR 12 WDMS binaries, i.e. the sum of all WDMS binary sub-samples. In this case, we do exclude duplicated targets that have been observed by different surveys. In the following section, we compare the different SDSS WDMS binary populations.

6 A COMPARISON OF THE DIFFERENT SDSS WDMS BINARY POPULATIONS

SDSS WDMS binaries come in different flavours. On the one hand, the majority of WDMS binaries are observed by SDSS simply because they have similar colours as quasars. These WDMS binaries include objects observed by the Legacy survey of SDSS I/II and objects observed by the BOSS survey of SDSS III. On the other hand, as can be seen in Fig. 6, a small number of WDMS binaries have been also observed by the SEGUE-2 survey of SDSS III. Finally, SDSS I/II WDMS binaries were additionally observed as part of our dedicated SEGUE survey (Rebassa-Mansergas et al. 2012a). Here, we compare these different SDSS WDMS binary populations. The stellar parameter cumulative distributions of white dwarf effective temperatures, surface gravities and masses, and secondary star spectral types for the different WDMS binary populations are shown in Fig. 7.

We run Kolmogorov–Smirnov (KS) tests to quantitatively compare the cumulative distributions (a χ^2 test in the case of the secondary star spectral types). The results are provided in Table 4. The probabilities are in most cases very low, thus indicating that the WDMS binaries of the four sub-samples are drawn from different parent populations. Indeed, there are no two sub-samples for which the obtained probabilities are above 15 per cent in all four cases (white dwarf effective temperature, mass, surface gravity and secondary star spectral type). The fact that the four sub-samples seem

to be statistically different is not too surprising and clearly indicates that the SDSS WDMS binary catalogue is heavily affected by selection effects of the different populations.

Legacy and BOSS WDMS binaries are most likely accidentally selected by the target selection algorithm of quasars and, in principle, we may expect these populations to be statistically similar. However, as we have already mentioned, the quasar selection algorithm has modified the limiting magnitude from $i < 19.1$ in SDSS I/II to $g < 22$ in SDSS III (Ross et al. 2012). Intrinsically faint WDMS binaries containing late-type companions and/or cool/high-mass white dwarfs are therefore more likely to be observed by the BOSS survey than the Legacy survey. Thus, the BOSS WDMS binary population displays a scarcity of low-mass ($M_{WD} \lesssim 0.5\,M_\odot$) as well as a higher fraction of cooler ($\lesssim 15\,000$ K) white dwarfs than the Legacy one (Fig. 6). Moreover, the secondary star spectral-type distribution of BOSS WDMS binaries presents a clear overabundance of late-type ($\geq$M6) companions as compared to the spectral-type distribution of Legacy WDMS binaries. This result suggests that the observed overall scarcity of SDSS WDMS binaries containing late-type companions (bottom-right panel of Fig. 6) is a simple consequence of selection effects incorporated by the SDSS selection criteria rather than an intrinsic physical property of these binaries.

SEGUE WDMS binaries were observed thanks to a dedicated survey performed by us to select objects with a strong contribution of the companion star (Rebassa-Mansergas et al. 2012a), hence they present statistical properties that are different from the other sub-samples. Interestingly, white dwarfs of both SEGUE and SEGUE-2 WDMS binaries seem to be of similar properties in terms of white dwarf mass and surface gravity (Table 4), although the number of SEGUE-2 systems is too low and these similarities need to be taken with caution.

SEGUE-2 WDMS binaries are selected as the result of a selection algorithm that aims at obtaining spectra of main-sequence stars and red giants. The colours of WDMS binaries are similar to those of single main-sequence stars only when the flux contribution of the white dwarf is small, i.e. the white dwarfs are expected to be cool and/or massive. Indeed, the white dwarf population of SEGUE-2 WDMS binaries is the coolest among the four sub-samples and the masses of 1/3 of the white dwarfs are $\geq 0.8\,M_\odot$ (Fig. 6). The

Table 5. 62 new SDSS PCEBs identified in this work. The Na I and H α columns indicate whether (1) or not (0) the system displays more than 3σ Na I and H α emission RV variation, respectively. WDMS binaries displaying only H α RV variation should be considered as PCEB candidates, except the eclipser SDSSJ093947.95+325807.3 (Section 8) and SDSSJ125645.47+252241.6 (see Fig. 8).

object	Na I	H α	object	Na I	H α	object	Na I	H α	object	Na I	H α
SDSSJ002547.09+134129.8	0	1	SDSSJ075356.37+233118.9	1	0	SDSSJ101642.94+044317.7	0	1	SDSSJ132040.27+661214.8	1	0
SDSSJ002926.82+252553.9	0	1	SDSSJ075335.00+510605.2	1	1	SDSSJ101739.89+594829.6	0	1	SDSSJ132830.92+125941.4	1	0
SDSSJ003239.97−002611.1	1	0	SDSSJ075835.11+482523.6	1	1	SDSSJ101954.64+531736.9	1	0	SDSSJ134100.03+602610.4	1	1
SDSSJ003336.49+004151.3	1	1	SDSSJ080003.86+503545.2	0	1	SDSSJ102750.05+271244.1	1	1	SDSSJ135039.54+261511.7	0	1
SDSSJ003402.18+325506.9	1	0	SDSSJ080235.69+525736.3	1	0	SDSSJ103008.34+393715.4	0	1	SDSSJ140138.47+121736.0	1	1
SDSSJ010428.86−000907.3	1	1	SDSSJ081409.82+531921.3	1	1	SDSSJ104606.35+583907.8	1	0	SDSSJ142522.83+210940.6	1	0
SDSSJ011845.09+303345.2	1	0	SDSSJ081942.67+542608.1	0	1	SDSSJ113829.09+202040.2	1	0	SDSSJ145443.65+570139.6	0	1
SDSSJ014745.02−004911.1	1	1	SDSSJ084028.85+501238.2	1	1	SDSSJ114349.96+501020.2	1	1	SDSSJ150605.75+265457.4	1	1
SDSSJ020756.15+214027.4	1	1	SDSSJ085515.48+280211.8	0	1	SDSSJ115411.77+543251.4	0	1	SDSSJ154145.39+412230.4	1	0
SDSSJ022405.97+002100.6	0	1	SDSSJ090451.86+453105.0	0	1	SDSSJ123234.07+601629.9	1	0	SDSSJ160553.66+085954.4	1	1
SDSSJ022436.80+005814.3	1	0	SDSSJ093155.66+394607.7	1	1	SDSSJ123406.86+443115.2	0	1	SDSSJ163831.67+292236.8	1	0
SDSSJ024310.60+004044.4	1	0	SDSSJ093947.95+325807.3	0	1	SDSSJ123642.17+005448.3	0	1	SDSSJ212320.23+054253.6	1	1
SDSSJ025301.60−013006.9	0	1	SDSSJ094853.94+573957.7	0	1	SDSSJ123902.93+654934.5	0	1	SDSSJ215819.27+000909.6	1	0
SDSSJ074244.88+421425.7	1	1	SDSSJ095043.94+391541.6	1	1	SDSSJ125645.47+252241.6	0	1	SDSSJ230202.49−000930.0	1	1
SDSSJ074301.93+410655.2	0	1	SDSSJ095250.46+155304.1	1	1	SDSSJ131630.63+612412.5	1	0	SDSSJ235524.29+044855.8	0	1
SDSSJ074605.00+480048.7	1	1	SDSSJ100811.87+162450.4	1	1						

secondary stars that are part of SEGUE-2 WDMS binaries seem to be of similar properties to those of the Legacy sample (Table 4).

7 RADIAL VELOCITIES AND IDENTIFICATION OF PCEBs

We here measure the Na I λλ 8183.27, 8194.81 absorption doublet and H α emission radial velocities (RV) from all SDSS WDMS binary spectra identified in this work. We analyse these RVs to detect close binaries, i.e. PCEBs, in our sample. That is, an object is considered to be a PCEB if we detect significant (more than 3σ) RV variation. If we do not detect RV variation we consider the system as a likely wide binary, as the probability exists for the RVs to sample the same orbital phase of a PCEB, in which case we would not detect RV variation (note also that low-inclination and long orbital period PCEBs are more difficult to identify).

We fit the Na I λλ 8183.27,8194.81 absorption doublet with a second-order polynomial plus a double-Gaussian line profile of fixed separation, and the H α emission line with a second-order polynomial plus a single-Gaussian line profile, as described in Rebassa-Mansergas et al. (2008) and Ren et al. (2013). Each SDSS spectrum is the result of combining several different exposures (hereafter sub-spectra), hence we measure the RVs from all available sub-spectra to thus increase the chances of detecting short orbital period PCEBs. However, we need to keep in mind that a large fraction of WDMS binaries found in this work are observed by the BOSS survey of SDSS and that their spectra are generally of low SN ratio (Fig. 2). Therefore, we expect a large fraction of BOSS WDMS binary sub-spectra to be of extremely low SN ratio and hence not suitable for measuring accurate RVs. Thus, we decide to measure the RVs from all combined spectra too. Measuring RVs from combined spectra has the main effect of decreasing the sensitivity to RV variations of very short orbital period PCEBs due to averaging out some orbital phase information.

We derive at least one Na I λλ 8183.27, 8194.81 absorption doublet and H α emission RV of an accuracy better than 20 km s^{-1} for 536 and 291 WDMS binaries, respectively. Since many of these WDMS binaries are not new identifications, we combine the RVs measured here to those available from our previous studies to analyse the number of close binaries, i.e. PCEBs, in the sample. We thus count 390 and 224 WDMS binaries with at least two available Na I and/or two available H α RV measurements, respectively, among which we detect 73 objects displaying more than 3σ Na I RV

variation and 66 systems displaying more than 3σ H α RV variation. If we only take into account systems with RVs taken on different nights[3] we derive a PCEB fraction of ∼27 per cent based on our Na I RV measurements, or ∼40 per cent based on our H α RV measurements. Whilst the former value is in agreement with the close binary fraction found by Nebot Gómez-Morán et al. (2011) of 21–24 per cent, the latter seems to be rather overestimated. This is a consequence of H α RVs being less robust as probe for RV variations most likely due to magnetic activity affecting the secondary stars, i.e. the M dwarfs may be relatively rapidly rotating for the H α emission to be patchy over their surface thus resulting in apparent RV variations (Rebassa-Mansergas et al. 2008). Hence, caution needs to be taken with those PCEBs displaying only H α emission RV variation. Two obvious exceptions here are SDSSJ093947.95+325807.3, which is found to be an eclipser (see Section 8), and SDSSJ125645.47+252241.6, for which we estimate its orbital period based on the H α RVs (see below). Excluding duplicate binaries that display both Na I and H α RV variation we end up with 98 unique PCEBs, of which 62 are new identifications. In Table 5, we provide the International Astronomical Union (IAU) names of the 62 new PCEBs.

We finally combine the RV information presented here with those RV values from our previous studies of all SDSS PCEBs and analyse the Scargle (1982) periodograms calculated from the RVs of each system to investigate the periodic nature of the RV variations. In three cases (SDSSJ073455.91+410537.4, SDSSJ102438.46+162458.2 and SDSSJ125645.47+252241.6) we are able to estimate the orbital periods based on the resulting periodograms (see left-hand panels of Fig. 8). We adopt the orbital periods as the values corresponding to the highest power in the periodograms and we then carry out sine-fits of the form

$$V_r = K_{\rm sec} \sin\left[\frac{2\pi(t - T_0)}{P_{\rm orb}}\right] + \gamma \tag{5}$$

to the RV data sets of each system, where γ is the systemic velocity, $K_{\rm sec}$ is the RV semi-amplitude of the companion star, T_0 is the time of inferior conjunction of the secondary star and $P_{\rm orb}$ is the orbital period. The RV values folded over the estimated orbital periods

---

[3] 230 WDMS binaries have at least two available Na I RVs taken on different nights, of which 62 display more than 3σ RV variation. 127 objects have at least two available H α emission RVs taken on different nights, of which 51 display more than 3σ RV variation.
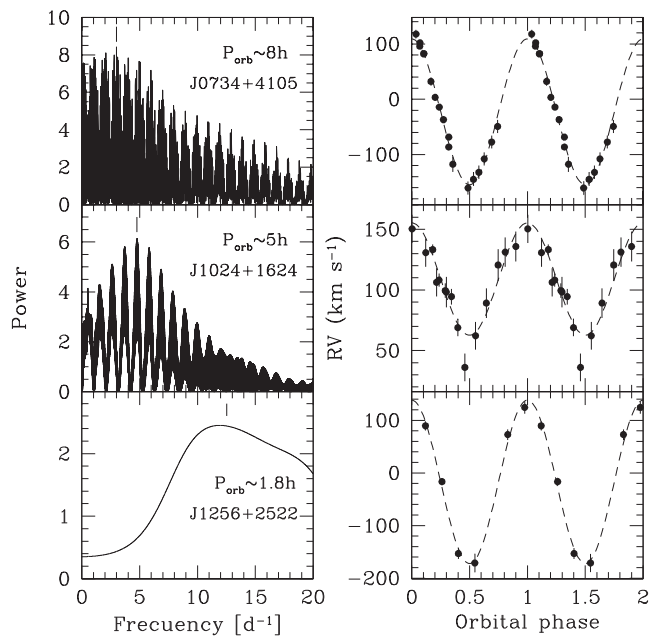
Figure 8. Left: Scargle periodograms calculated from the RV variations measured from the Na I absorption doublet in SDSSJ073455.91+410537.4 and SDSSJ102438.46+162458.2 and from the H α emission line in SDSSJ125645.47+252241.6. The most likely orbital periods (i.e. the values with the highest power) are indicated by tick marks. Right: the RV measurements folded over the adopted orbital periods of the systems.

Table 6. Estimated orbital periods P_{orb}, semi-amplitudes K_{sec} and systemic velocities γ. It is worth noting the high systemic velocity of SDSSJ102438.46+162458.2.

Object	P_{orb} (h)	K_{sec} (km s^{-1})	γ (km s^{-1})
SDSSJ073455.91+410537.4	8	132	−23
SDSSJ102438.46+162458.2	5	46	109
SDSSJ125645.47+252241.6	1.8	155	−17

obtained f the sine-fits are provided on the right-hand panels of Fig. 8. The estimated parameters resulting from these fits are reported in Table 6.

The RVs measured in this section, the heliocentric Julian dates of each observation and information on whether the systems are PCEBs or wide WDMS binaries can be found in our web site http://www.sdss-wdms.org.

8 ECLIPSING WDMS BINARIES

In this final section, we search for eclipsing WDMS binaries using photometry from the Catalina Sky Survey (CSS) and Catalina Real Time Transient Survey (CRTS; Drake et al. 2009). We followed the same approach detailed in Parsons et al. (2013) and Parsons et al. (2015) whereby we selected all WDMS binaries with magnitudes of $r < 19$ and re-reduced the raw CSS data ourselves to more easily identify very deeply eclipsing systems and remove any contaminated exposures. Out of the 1177 and 91 WDMS binaries and candidates identified here, only 314 were bright enough and with sufficient coverage to search for eclipses, i.e. a fraction of ∼25 per cent. This low percentage is mainly due to the fact that a large fraction of the WDMS binaries identified in this work were observed by the BOSS survey of SDSS of limiting magnitude $g < 22.0$. That is, many WDMS

binaries do not survive the $r < 19$ cut we applied. We identified seven eclipsing systems, however all of these were previously known: SDSSJ011009.14+132615.66 (Pyrzas et al. 2009), SDSSJ093947.92+325807.59, SDSSJ095719.24+234240.69, SDSSJ141057.72-020236.48, SDSSJ142355.06+240924.43, SDSSJ145634.25+161138.11 (Drake et al. 2010) and SDSSJ141536.38+011718.59 (Green, Richstone & Schmidt 1978). We also discovered that SDSSJ074244.91+421426.17 is in fact a MS+MS eclipsing binary as revealed by a deep secondary eclipse and thus exclude it from our list. Hence, the total number of SDSS WDMS binaries is 3294, 646 of which are new. The number of eclipsing systems among our sample is consistent with previous results indicating that ∼10 per cent of PCEBs – which make up roughly one fourth of WDMS binaries (Schreiber et al. 2010; Nebot Gómez-Morán et al. 2011; Rebassa-Mansergas et al. 2011) – are eclipsing systems (Parsons et al. 2013).

9 SUMMARY AND CONCLUSIONS

The spectroscopic catalogue of SDSS WDMS binaries now contains 3294 systems from DR 12. 979 are additions from the here presented work, 646 of which have not been published before. This is by far the largest, most complete and most homogeneous catalogue of compact binaries currently available. We have provided stellar parameters (white dwarf effective temperatures, surface gravities and masses, and secondary star spectral types) and RVs for the here identified WDMS binaries. We have also applied 3D corrections to the derived white dwarf parameters of all SDSS WDMS binaries. The stellar parameter distributions corresponding to WDMS binaries observed by the different surveys of SDSS (Legacy, BOSS, SEGUE, SEGUE-2) are statistically different due to the different target selection criteria used. This clearly reveals that the SDSS WDMS binary sample, though being the largest, is heavily affected by selection effects. In particular, we find indications for these selection effects to be responsible for the overall scarcity of observed SDSS WDMS binaries containing late-type (≥M6) companions. The RVs of 98 of our here studied SDSS WDMS binaries (62 of which are new identifications) display significant variation and we flag these systems as close binaries. For three of them the RV data are sufficient to estimate their orbital periods. We have also identified seven WDMS binaries as eclipsing, although all of them have been published before.

The SDSS WDMS binary catalogue is a superb sample that is being used to tackle many different open problems in modern astrophysics, ranging from constraining the physical properties of low-mass main-sequence stars and white dwarfs to improving our understanding of close compact binary evolution, among others.

SDSS-III is managed by the Astrophysical Research Consortium for the Participating Institutions of the SDSS-III Collaboration including the University of Arizona, the Brazilian Participation Group, Brookhaven National Laboratory, Carnegie Mellon University, University of Florida, the French Participation Group, the German Participation Group, Harvard University, the Instituto de Astrofisica de Canarias, the Michigan State/Notre Dame/JINA Participation Group, Johns Hopkins University, Lawrence Berkeley National Laboratory, Max Planck Institute for Astrophysics, Max Planck Institute for Extraterrestrial Physics, New Mexico State University, New York University, Ohio State University, Pennsylvania State University, University of Portsmouth, Princeton University, the Spanish Participation Group, University of Tokyo, University of Utah, Vanderbilt University, University of Virginia, University of Washington and Yale University.

REFERENCES

Abazajian K. N. et al., 2009, ApJ, 182, 543
Adelman-McCarthy J. K. et al., 2008, ApJS, 175, 297
Ahn C. P. et al., 2014, ApJ, 211, 17
Alam S. et al., 2015, ApJS, 219, 12
Andrews J. J., Price-Whelan A. M., Agüeros M. A., 2014, ApJ, 797, L32
Bergeron P., Wesemael F., Beauchamp A., 1995, PASP, 107, 1047
Camacho J., Torres S., García-Berro E., Zorotovic M., Schreiber M. R., Rebassa-Mansergas A., Nebot Gómez -Morán A., Gänsicke B. T., 2014, A&A, 566, A86
Chui C. K., 1992, Wavelets: A Tutorial in Theory and Applications. Academic Press, New York
Cui X.-Q. et al., 2012, Res. Astron. Astrophys., 12, 1197
Davis P. J., Kolb U., Willems B., 2010, MNRAS, 403, 179
Dawson K. S. et al., 2013, AJ, 145, 10
Drake A. J. et al., 2009, ApJ, 696, 870
Drake A. J. et al., 2010, preprint (arXiv:e-prints)
Duquennoy A., Mayor M., 1991, A&A, 248, 485
Dye S. et al., 2006, MNRAS, 372, 1227
Eisenstein D. J. et al., 2011, AJ, 142, 72
Farihi J., Hoard D. W., Wachter S., 2010, ApJ, 190, 275
Ferrario L., 2012, MNRAS, 426, 2500
Gentile Fusillo N. P., Gänsicke B. T., Greiss S., 2015, MNRAS, 448, 2260
Green R. F., Richstone D. O., Schmidt M., 1978, ApJ, 224, 892
Hermes J. J. et al., 2015, MNRAS, 451, 1701
Hewett P. C., Warren S. J., Leggett S. K., Hodgkin S. T., 2006, MNRAS, 367, 454
Kepler S. O. et al., 2015, MNRAS, 446, 4078
Kepler S. O. et al., 2016, MNRAS, 455, 3413
Kilic M., Brown W. R., Gianninas A., Hermes J. J., Allende Prieto C., Kenyon S. J., 2014, MNRAS, 444, L1
Koester D., 2010, Mem. Soc. Astron. Ital., 81, 921
Koester D., Kepler S. O., Kleinman S. J., Nitta A., 2009, J. Phys. Conf. Ser., 172, 012006
Lawrence A. et al., 2007, MNRAS, 379, 1599
Li L., Zhang F., Han Q., Kong X., Gong X., 2014, MNRAS, 445, 1331
Liu X.-W. et al., 2014, in Feltzing S., Zhao G., Walton N. A., Whitelock P., eds, Proc. IAU Symp. 298, Setting the Scene for Gaia and LAMOST. Cambridge Univ. Press, Cambridge, p. 310
Luo A.-L. et al., 2012, Res. Astron. Astrophys., 12, 1243
Manser C. J., Gänsicke B. T., 2014, MNRAS, 442, L23
Marsh T. R. et al., 2014, MNRAS, 437, 475
Martin D. C. et al., 2005, ApJ, 619, L1
Morrissey P. et al., 2005, ApJ, 619, L7
Nebot Gómez-Morán A. et al., 2009, A&A, 495, 561
Nebot Gómez-Morán A. et al., 2011, A&A, 536, A43
Nelemans G., Siess L., Repetto S., Toonen S., Phinney E. S., 2016, ApJ, 817, 69
Parsons S. G. et al., 2012a, MNRAS, 419, 304
Parsons S. G. et al., 2012b, MNRAS, 420, 3281
Parsons S. G. et al., 2013, MNRAS, 429, 256
Parsons S. G. et al., 2014, MNRAS, 438, L91
Parsons S. G. et al., 2015, MNRAS, 449, 2194
Pyrzas S. et al., 2009, MNRAS, 394, 978
Pyrzas S. et al., 2012, MNRAS, 419, 817
Raghavan D. et al., 2010, ApJ, 190, 1
Rebassa-Mansergas A., Gänsicke B. T., Rodríguez-Gil P., Schreiber M. R., Koester D., 2007, MNRAS, 382, 1377
Rebassa-Mansergas A. et al., 2008, MNRAS, 390, 1635
Rebassa-Mansergas A., Gänsicke B. T., Schreiber M. R., Koester D., Rodríguez-Gil P., 2010, MNRAS, 402, 620
Rebassa-Mansergas A., Nebot Gómez-Morán A., Schreiber M. R., Girven J., Gänsicke B. T., 2011, MNRAS, 413, 1121
Rebassa-Mansergas A., Nebot Gómez-Morán A., Schreiber M. R., Gänsicke B. T., Schwope A., Gallardo J., Koester D., 2012a, MNRAS, 419, 806
Rebassa-Mansergas A. et al., 2012b, MNRAS, 423, 320
Rebassa-Mansergas A., Schreiber M. R., Gänsicke B. T., 2013a, MNRAS, 429, 3570
Rebassa-Mansergas A., Agurto-Gangas C., Schreiber M. R., Gänsicke B. T., Koester D., 2013b, MNRAS, 433, 3398
Ren J., Luo A., Li Y., Wei P., Zhao J., Zhao Y., Song Y., Zhao G., 2013, AJ, 146, 82
Ren J. J. et al., 2014, A&A, 570, A107
Renedo I., Althaus L. G., Miller Bertolami M. M., Romero A. D., Córsico A. H., Rohrmann R. D., García-Berro E., 2010, ApJ, 717, 183
Ross N. P. et al., 2012, ApJ, 199, 3
Scargle J. D., 1982, ApJ, 263, 835
Schreiber M. R., Gänsicke B. T., Southworth J., Schwope A. D., Koester D., 2008, A&A, 484, 441
Schreiber M. R. et al., 2010, A&A, 513, L7
Schreiber M. R., Zorotovic M., Wijnen T. P. G., 2016, MNRAS, 455, L16
SDSS-III Collaboration et al., 2014, ApJS, 211, 17
Smolčić V. et al., 2004, ApJ, 615, L141
Toonen S., Nelemans G., 2013, A&A, 557, A87
Tremblay P.-E., Ludwig H.-G., Steffen M., Bergeron P., Freytag B., 2011, A&A, 531, L19
Tremblay P.-E., Ludwig H.-G., Steffen M., Freytag B., 2013, A&A, 559, A104
Webbink R. F., 2008, in Milone E. F., Leahy D. A., Hobill D. W., eds, Astrophysics and Space Science Library, Vol. 352, Short-Period Binary Stars: Observations, Analyses, and Results. Springer-Verlag, Berlin, p. 233
Willems B., Kolb U., 2004, A&A, 419, 1057
Yanny B. et al., 2009, AJ, 137, 4377
York D. G. et al., 2000, AJ, 120, 1579
Yuan H.-B. et al., 2015a, MNRAS, 448, 855
Yuan H., Liu X., Xiang M., Huang Y., Chen B., Wu Y., Hou Y., Zhang Y., 2015b, ApJ, 799, 135
Zorotovic M., Schreiber M. R., 2013, A&A, 549, A95
Zorotovic M., Schreiber M. R., Gänsicke B. T., Nebot Gómez-Morán A., 2010, A&A, 520, A86
Zorotovic M. et al., 2011a, A&A, 536, L3
Zorotovic M., Schreiber M. R., Gänsicke B. T., 2011b, A&A, 536, A42
Zorotovic M., Schreiber M. R., García-Berro E., Camacho J., Torres S., Rebassa-Mansergas A., Gänsicke B. T., 2014, A&A, 568, A68

SUPPORTING INFORMATION

Additional Supporting Information may be found in the online version of this article:

t-new-wdms.dat

(http://www.mnras.oxfordjournals.org/lookup/suppl/doi:10.1093/mnras/stw554/-/DC1).

Please note: Oxford University Press is not responsible for the content or functionality of any supporting materials supplied by

the authors. Any queries (other than missing material) should be directed to the corresponding author for the paper.

APPENDIX A: NOTES ON INDIVIDUAL SYSTEMS

SDSSJ003336.49+004151.3, SDSSJ014745.02-004911.1, SDSSJ024310.60+004044.4, SDSSJ132040.27+661214.8 and SDSSJ132830.92+125941.4: these five WDMS binaries have been found to display Na I RV variation (Section 7). However, they were flagged as wide WDMS binaries in our previous studies (Schreiber et al. 2010; Rebassa-Mansergas et al. 2011). This may indicate that these binaries have relatively long orbital periods of a few hundred of days (as the spectra analysed in this work are separated by this amount of time from the spectra analysed in our previous studies), or simply that our previous RV measurements sampled always the same orbital phases.

SDSSJ013714.97+210220.0 and SDSSJ100615.27+242612.1: we classify SDSS0137 as a new low-accretion rate polar (LARP). The SDSS spectrum displays clear cyclotron emission at ~4800 Å. We identify two emission bumps at ~4400 and ~6500 Å in the SDSS spectrum of SDSSJ1006 that may also arise as a consequence of cyclotron emission. Hence, SDSSJ1006 may also be a LARP. The SDSS spectra of the two systems are shown in Fig. A1.

SDSSJ073953.89+392732.5: we classify the main-sequence companion as a metal-poor subdwarf.

SDSSJ081647.38+534017.8, SDSSJ083938.54+395440.5, SDSSJ101819.47+174702.34 and SDSSJ161213.77+163906.2: these four WDMS binaries may be eclipsing. Two SDSS spectra of SDSSJ0816 reveal the presence and absence of the white dwarf, respectively, thus suggesting the second spectrum was obtained during an eclipse (see Fig. A2). However, it is important to mention that the Na I RVs measured from the SDSS spectra do not reveal any sign of variation. The SDSS spectra and *ugriz* fluxes derived from SDSS photometry of SDSSJ0839 and SDSSJ1612 are shown in Fig. A3. Inspection of the figure clearly reveals that the *u*-band fluxes (also the *z*-band flux for SDSSJ0839) do not match the spectra. We consider this may be a consequence of the SDSS photometry being obtained during eclipses, i.e. the *u*-band
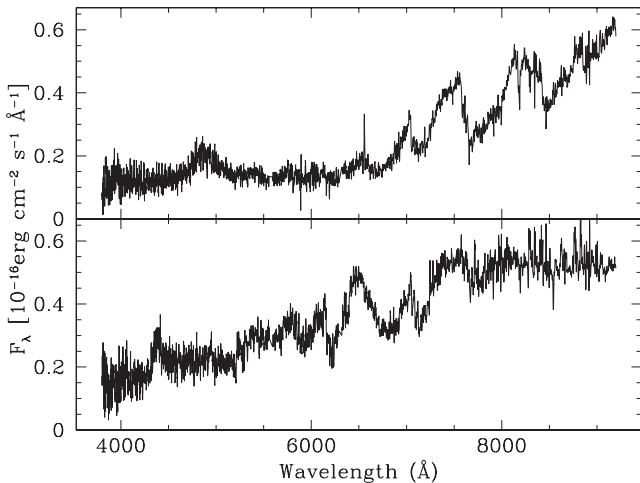

Figure A1. Top panel: SDSS spectrum of SDSSJ013714.97+210220.0, a new LARP. Bottom panel: SDSS spectrum of SDSSJ100615.27+242612.1, a new candidate LARP.
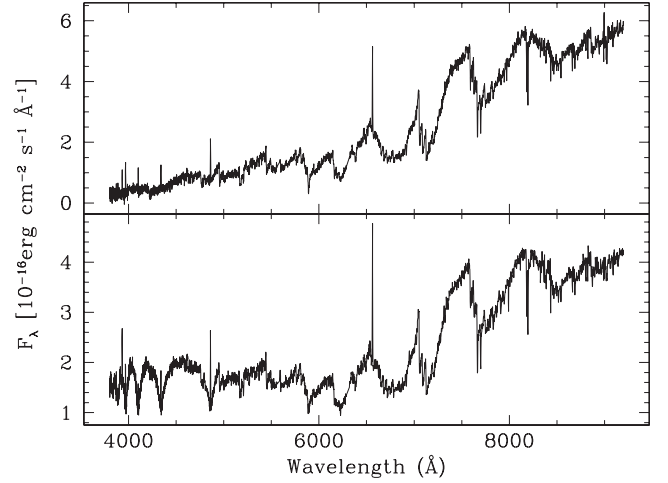

Figure A2. Two SDSS spectra of SDSSJ081647.38+534017.8. The white dwarf is clearly visible in the bottom-panel spectrum, but is completely absent in the top-panel spectrum. This may be because the top-panel spectrum was taken during an eclipse. Puzzlingly, the Na I RVs measured from the SDSS spectra do not show any variation.
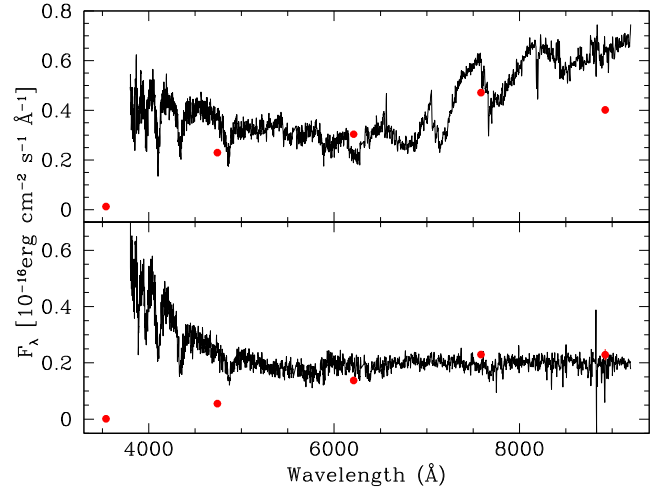

Figure A3. SDSS spectra of SDSSJ083938.54+395440.5 (top panel) and SDSSJ161213.77+163906.2 (bottom panel). *ugriz* fluxes derived from the available SDSS photometry are shown as red solid dots.

photometry correspond to that of the main-sequence companions. Finally, we detect several faint points in the Catalina light curve of SDSSJ1018, indicating that it may well be eclipsing, however there is insufficient data to confirm this or determine its period.

SDSSJ123931.98+210806.2: the SDSS spectrum shows a DA white dwarf, a late-type secondary star and Balmer lines in emission. Originally classified as a WDMS binary, this object was excluded from our sample after we realized it is the cataclysmic variable IR Com (Manser & Gänsicke 2014). The SDSS spectrum was taken in a low state.

SDSSJ213408.21+065057.5: the SDSS spectrum displays the typical features of a DO degenerate and an early-type secondary star. H α is in emission.

This paper has been typeset from a TEX/LATEX file prepared by the author.